DNA-methylation changes have been observed in cancer [11,12]. One is a global hypomethylation associated with increased chromosomal instability, the reactivation of transposable elements, and loss of imprinting. The other is hypermethylation of CpG islands located in promoter regions of tumor suppressor genes that has conventionally been associated with transcriptional silencing in cancer. These aberrant DNA methylations are thought to be closely related to the development of cancer. Therefore, the identification of specific DNA methylation markers would be helpful for understanding the pathogenetic mechanism as well as for developing new therapeutic strategies. In Wilms' tumor, hypermethylation of *HACE1*, *RASSF1A* and *SIM1* and hypomethylation of *GRIPR* were reported [13–16], whereas the DNA methylation analysis in pediatric renal sarcomas including RTK, CCSK has not been reported yet.

In an attempt to investigate the characteristics of DNA methylation of pediatric sarcomas including CCSK, RTK, and ESFT, we performed DNA methylation analysis using Illumina Infinium HumanMethylation27. In this paper, we demonstrated that each sarcoma had a distinct DNA methylation profile and could be classified by the methylation pattern of a set of specific genes. We further proposed a convenient assay for the differential diagnosis of CCSK from other pediatric renal tumor.

Materials and Methods

Ethics Statement

This study was approved by the ethics committee/IRB at the National Center for Child Health and Development, and written informed consent was obtained from parents for samples from JWiTS. Since written informed consent was not obtained in a subset of samples collected before 2001, the identifying information for them was removed before analysis, in accordance with the Ethical Guideline for Clinical Research enacted by the Japanese Government. The ethics committee/IRB approved the waiver of written informed consent for latter samples.

Table 2. The number of hyper- and hypomethylated genes in comparison with non-neoplastic kidney.

	CpG island probe	
	Hypermethylated	**Hypomethylated**
CCSK	490 probes (437 genes)	46 probes (36 genes)
RTK	130 probes (107 genes)	65 probes (62 genes)
ESFT	66 probes (58 genes)	55 probes (46 genes)
	Non-CpG island probe	
	Hypermethylated	**Hypomethylated**
CCSK	184 probes (166 genes)	117probes (112 genes)
RTK	179 probes (160 genes)	320probes (275 genes)
ESFT	113 probes (101 genes)	136probes (124 genes)

Hypermethylation: difference of average β-value >0.3. Hypomethylation: difference of average β-value<−0.3.
doi:10.1371/journal.pone.0062233.t002

Clinical Materials

Clinical specimens from pediatric patients, including 6 each with RTK and Ewing's sarcoma, 21 with CCSK, 9 with CMN, and 41 with Wilms' tumor, used in this study were selected from the files of specimens collected in our laboratory between 1985 and 2001, and the JWiTS (Japan Wilms Tumor Study). In each case, the pathological diagnosis was confirmed by J.H. and H.O. based on morphological observations and the immunophenotypic characteristics. Three non-neoplastic kidney (NK) tissues were obtained from the non-tumorous part of the above specimens.

Sample Preparation

Each disease tissue was evaluated by preparing frozen section and the neoplastic cells accounted for more than 80% of viable

Table 1. Primers used for MassARRAY.

Primer name	5′ - 3′ sequence
ADRA1D_F	aggaagagagTGGTAGGTAATTTGTTTGTTATTTTTTT
ADRA1D_R	cagtaatacgactcactatagggagaaggctCTTCCAACCCAACAAAAACCCTA
ALDOC_F	aggaagagagTTGAATTTGGGTATTTTGAAGATGT
ALDOC_R	cagtaatacgactcactatagggagaaggctCAAATAAAACTACAACCCTAACTCCC
CREG1_F	aggaagagagGTGAGTAATTTGTAGGTGAGTTGGG
CREG1_R	cagtaatacgactcactatagggagaaggctCCACTACACTCCAACCTAAACCA
MGMT_F	aggaagagagTGAGATTGTTAGAGTGTGTTTTTGG
MGMT_R	cagtaatacgactcactatagggagaaggctTCCACTCAAACCAACTAAATTACCTA
PKN1_F	aggaagagagGGTTTTTTTTGGAGAATTAGAAGGG
PKN1_R	cagtaatacgactcactatagggagaaggctCCAACCACCATACAAAAAAATAAAA
PTEN_F	aggaagagagGGGGTTGTAAATAGATTTGATAGGTT
PTEN_R	cagtaatacgactcactatagggagaaggctAAAAAAAATCCCCAAACTAATACCA
THBS1_F	aggaagagagGGAGAGAGGAGTTTAGATTGGTTTT
THBS1_R	cagtaatacgactcactatagggagaaggctACCTTACCCTAAAAAATCCTCCAAC
VHL_F	aggaagagagTTTTGGGGAGATTGATAGATGTAAA
VHL_R	cagtaatacgactcactatagggagaaggctAACCACTTAACCCCAAATAACAAAT

F, forward; R, reverse. Lower case letters indicate tag sequences.
doi:10.1371/journal.pone.0062233.t001

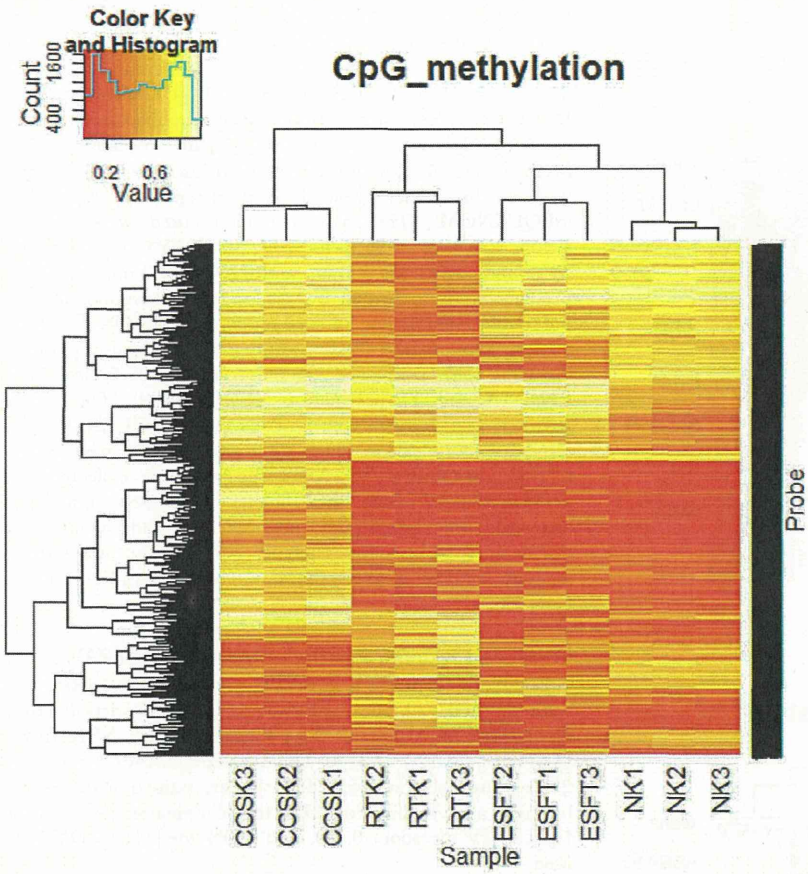

Figure 1. Hierarchical cluster analysis of methylation value (β) in Infinium assay on pediatric tumors. Two-way hierarchical cluster analysis of the methylation level of 1,494 probes (rows, equivalent to hyper- and hypomethylated genes shown in Table 2) and three cases for each of clear cell sarcoma of the kidney (CCSK), rhabdoid tumor of the kidney (RTK), the Ewing's sarcoma family of tumors (ESFT), and non-neoplastic kidney (NK) (columns) were performed using hclust in the R clustering package. The β-values ranged from 0 (unmethylated) to 1 (fully methylated) on a continuous scale.
doi:10.1371/journal.pone.0062233.g001

cells in each sample. The pathologic images of the disease tissues were presented in Figure S1. Genomic DNA was extracted from above evaluated fresh-frozen tissues using the illustra tissue & cells genomicPrep Mini Spin kit (GE Healthcare Bio-Sciences UK Ltd, Chalfont, UK) according to the manufacturer's instructions. The quantity of DNA was assessed by Quant-iT Pico-Green dsDNA Reagent and Kits (Life Technologies Corporation, Carlsbad, CA, USA) and the quality was assessed by agarose gel electrophoresis.

Table 3. The number of specifically methylated genes compared with other each of tumors and non-neoplastic kidney.

	Hypermethylation	Hypomethylation
CCSK	270 genes	28 genes
RTK	65 genes	155 genes
ESFT	7 genes	35 genes

Hypermethylation: difference of average β-value >0.3. Hypomethylation: difference of average β-value<−0.3.
doi:10.1371/journal.pone.0062233.t003

Bisulfite Conversion

Starting from 1 μg of genomic DNA, bisulfite conversion of genomic DNA was performed using the Epitect Bisulfite kit (QIAGEN Inc., Valencia, CA, USA) and EZ DNA Methylation Kit (Zymo Research, Irvine, CA, USA) for the Illumina Infinium Methylation Assay and SEQUENOM MassARRAY, respectively, according to the manufacturer's protocol.

Infinium Methylation Assay

Illumina Infinium HumanMethylation27 (Illumina, Inc., San Diego, CA, USA), containing the 27,578 CpG sites, spanning 14,495 genes, was used for methylation analysis. The bisulfite converted DNA was processed on the chip according to the Illumina protocol. The BeadChips were scanned using iScan system. Our data of Infinium assay have been deposited on Gene Expression Omnibus (GEO) database at the National Center for Biotechnology Information (NCBI, http://www.ncbi.nlm.nih.gov/geo/, series accession number GSE44847). The β-value and the detection p-value for each locus were calculated using GenomeStudio v2010.1. β-value, a ratio of methylated probe signal intensity to sum of methylated and unmethylated probe signal intensities, was used to estimate the methylation

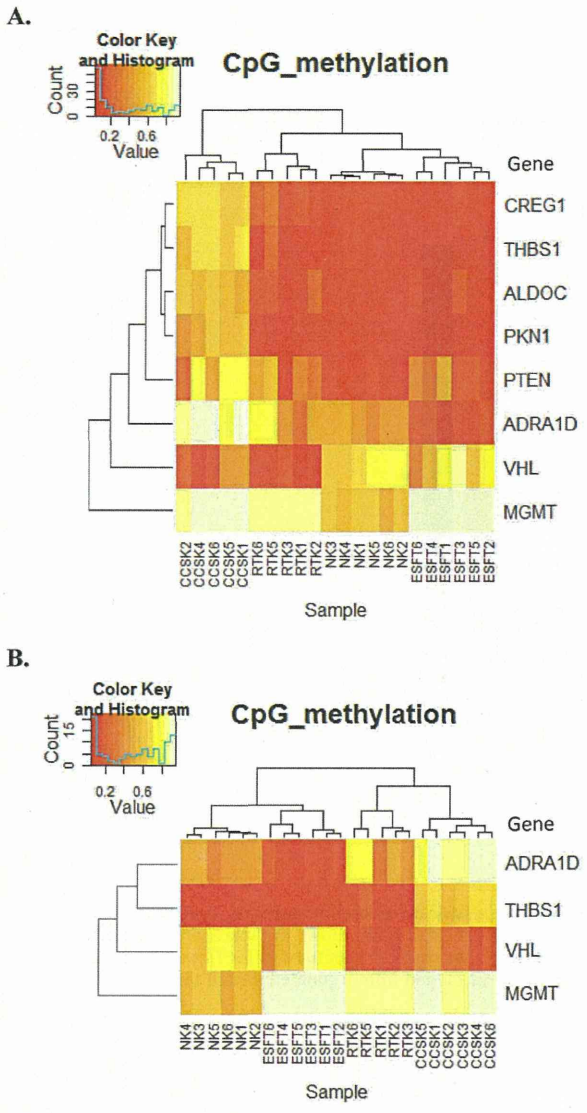

Figure 2. Hierarchical cluster analysis of methylation level of CpG analyzed by MassARRAY. (A) Based on the results indicated in Figure 1, 8 genes were selected as described in the text and analyzed by MassARRAY. Two-way hierarchical cluster analysis was performed using the CpG methylation average of all CpG that have passed QC from each gene. Two cases (RTK4 and CCSK3) showed failed analysis of some CpG sites, and were excluded from hierarchical analysis. (B) Four genes were further selected, and cluster analysis using the methylation average was performed as in (A). CCSK3 was successfully analyzed in all four genes, and included in this analysis.
doi:10.1371/journal.pone.0062233.g002

level of the target locus. Detection p-value is computed from the background model characterizing the chance that the target sequence signal was distinguishable from negative controls. The obtained data were filtered by exclusion of the probes with a detection p-value>0.05 from all probes and SD>0.2 within each entity. The numbers of the detected CpG sites for each sample and filtering process were shown in Table S1. As a result, 23,700 probes (13,385 genes) remained.

EPITYPER Assay (MassARRAY)

The SEQUENOM EpiTYPER assay was performed according to the protocol recommended by the manufacturer. Using the Complete PCR Reagent Set (SEQUENOM Inc., San Diego, CA, USA), target regions were amplified from bisulfite-converted DNAs using the primer pairs containing a T7-promoter tag to allow further *in vitro* transcription. The primers used in this study (Table 1) were designed by EpiDesigner (SEQUENOM). The cycle conditions used were: 95°c for 4 min, 45 cycles of 95°C for 20 s, 56°C (65°C for *CREG1*) for 30 s. and, 95°C for 1 min, and 72°C for 3 min. The PCR products were confirmed by agarose gel electrophoresis. After the dephosphorylation of unincorporated dNTPs by shrimp alkaline phosphatase (SAP) (SEQUENOM), transcription and digestion were performed simultaneously at 37°C for 3 h by RNase A and T7 polymerase (SEQUENOM). The cleavage reactants were purified with CLEAN resin (SEQUENOME) and dispensed onto silicon chips preloaded with matrix (Spectro-CHIPS, SEQUENOM). Mass spectra were collected using a MassARRAY mass spectrometer (Bruker-Sequenom) and analyzed using proprietary peak picking and signal-to-noise calculations (Sequenom Epityper v1.0.5). In MassARRAY analysis, initially, quality control (QC) was performed in each CpG site.

Combined Bisulfite Restriction Analysis (COBRA)

Bisulfite PCR products of *THBS1* produced as described above were digested with the methylation-sensitive restriction enzyme HpyCH4IV (5′-ACGT-3′) (New England Biolabs, NEB, Ipswich, MA, USA) for 12 h at 37°C The digested DNA was separated on 2% agarose gels in 0.5× TBE buffer, stained with ethidium bromide, and visualized on a UV transilluminator. As a control of HpyCH4IV digestion, 0, 50, and 100% methylated DNA were used.

Statistical Analysis

Two-way hierarchical cluster analyses of Infinium assay and MassARRAY were performed using hclust in the R clustering package with Euclidean metric and complete linkage for statistical computing.

Results

DNA methylation profiling of 3 each of CCSK, RTK, ESFT and NK, 12 samples in total, were performed using Infinium HumanMethylation27. First, we analyzed the general methylation status of each tumor group by defining hyper- and hypomethylated CpG sites in each tumor group as those with average β-value differences of >0.3 and <−0.3 compared to NK, respectively. The numbers of selected hyper- and hypomethylated CpG probes in each tumor are listed in Table 2. Among them, the number of selected hypermethylated CpG probes mapped on the CpG island in CCSK, RTK, and ESFT were 490, 130, and 66, respectively, while those of hypomethylated non-CpG probes were 117, 320, and 136, respectively (Table 2).

To test whether the tumors can be distinguished by the methylation level, we performed two-way hierarchical cluster analysis of methylation patterns using hyper- and hypomethylated sites (1,494 probes; equivalent to 1,281 genes selected in Table 2). As shown in Figure 1, each case in the same tumor was clustered in the same group, indicating the tumor-type-dependent methylation pattern of the selected probes.

To further select marker genes for methylation-based tumor-type classification, we defined tumor-specific differentially meth-

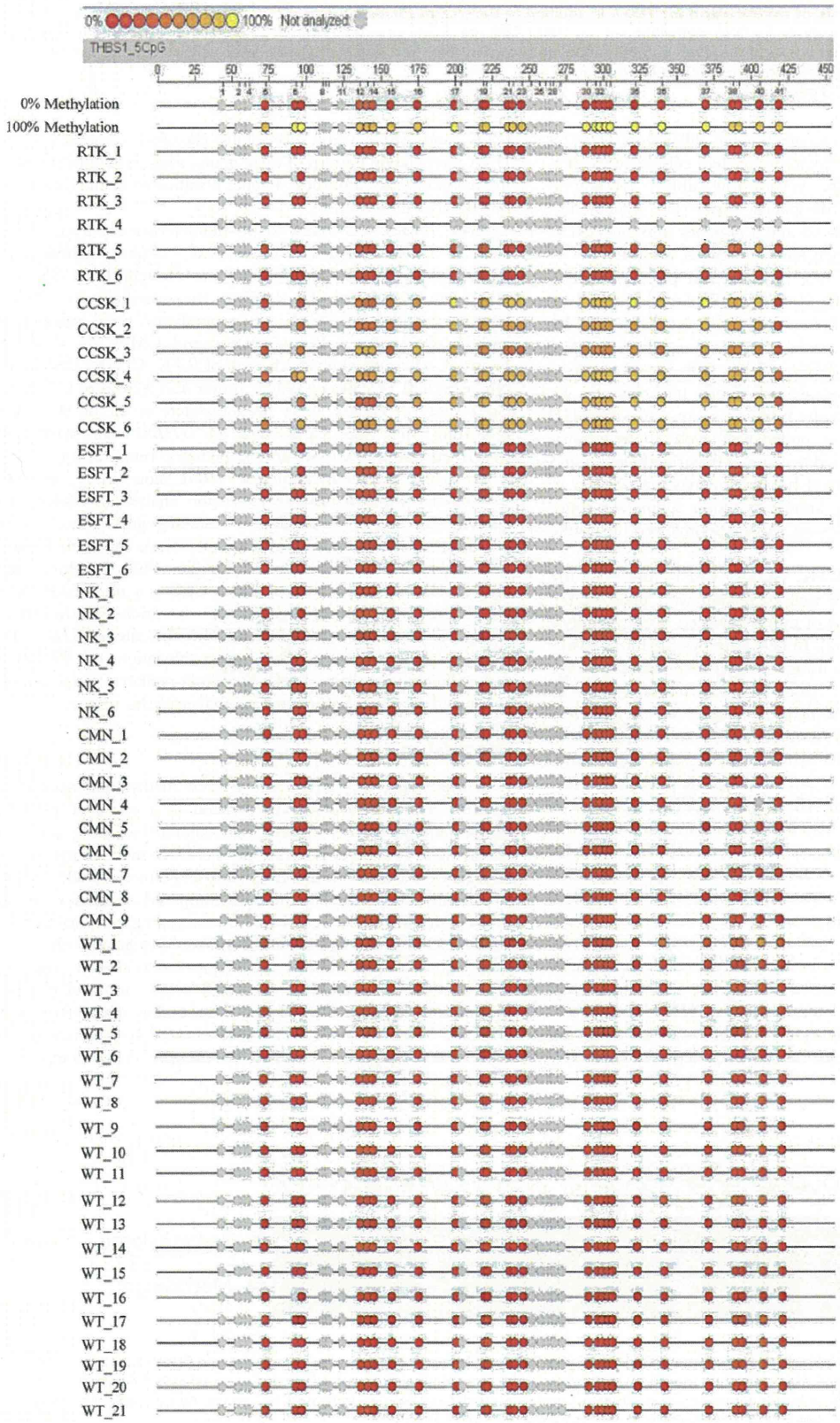
0%
100%
Not analyzed
THBS1_5CpG
0 25 50 75 100 125 150 175 200 225 250 275 300 325 350 375 400 425 450
0% Methylation
100% Methylation
RTK_1
RTK_2
RTK_3
RTK_4
RTK_5
RTK_6
CCSK_1
CCSK_2
CCSK_3
CCSK_4
CCSK_5
CCSK_6
ESFT_1
ESFT_2
ESFT_3
ESFT_4
ESFT_5
ESFT_6
NK_1
NK_2
NK_3
NK_4
NK_5
NK_6
CMN_1
CMN_2
CMN_3
CMN_4
CMN_5
CMN_6
CMN_7
CMN_8
CMN_9
WT_1
WT_2
WT_3
WT_4
WT_5
WT_6
WT_7
WT_8
WT_9
WT_10
WT_11
WT_12
WT_13
WT_14
WT_15
WT_16
WT_17
WT_18
WT_19
WT_20
WT_21

Figure 3. MassARRAY analysis of methylation in *THBS1*. In addition to the 6 cases for each tumor group, 9 and 21 cases of CMN and Wilms' tumor (WT), respectively, were analyzed for DNA methylation of the *THBS1* CpG site, as in Figure 2A. Different colored of circles mark the position of CpG within the sequence (straight line) and the levels of methylation are shown in color (red, low methylation level; yellow, high methylation level). Gray circles represent the unanalyzed CpG sites. WT: Wilms' tumor.
doi:10.1371/journal.pone.0062233.g003

ylated genes as those with average β-value differences of >0.3 (hypermethylated) or <−0.3 (hypomethylated) compared to each of other tumor groups and NK. As shown in Table 3, 270 and 28 genes were identified as CCSK-specific hyper- and hypomethylated genes, respectively, while 65 and 155 genes were selected as RTK-specific hyper- and hypomethylated genes, respectively.

Employing MassARRAY, next we analyzed the surrounding CpG of some specific probes filtered in Table 2, in detail to validate the results of an Infinium assay and further search for candidate genes for a differential diagnostic marker of renal sarcomas. Genes *ALDOC*, *CREG1*, *PKN1*, and *Thrombospondin-1 (THBS1)* were selected because of their tendency to be hypermethylated in CCSK by the Infinium assay, while *ADRA1D* was selected because of distinct methylation levels among tumors. *MGMT* and *PTEN* were selected because of hypermethylation in 3 tumors, while *VHL* was selected because of hypomethylation in CCSK and RTK. These are known as tumor suppressor genes and these methylation changes are reportedly involved in specific tumors. [17,18].

We analyzed 6 each of RTK, CCSK, ESFT, and NK, the results of MassARRAY were well correlated with those of the Infinium assay, and each type of tumor revealed a specific DNA methylation pattern (Figure S2). In fact, when we performed two-way hierarchic cluster analysis using the CpG methylation average derived from the results, the cases for each tumor type were successfully classified into the same group (Figure 2A). As shown in Figure 2A, *CREG1*, *ALDOC*, *THBS1*, and *PKN1* were hypermethylated in CCSK, whereas RTK, ESFT, and NK were hypomethylated at specific CpG loci, as analyzed by the Infinium assay. *PTEN* was hypomethylated in NK, while variably methylated in sarcoma cases. *ADRA1D* was also hypermethylated in CCSK but hypomethylated in ESFT in comparison with NK, whereas variably methylated in RTK. Although *VHL* was hypomethylated in CCSK and RTK, it was hypermethylated in NK (Figure S3 and Figure S4). *MGMT* was hypermethylated in tumor groups compared to NK.

To distinguish these tumors by the DNA methylation pattern more simply, we further selected four genes characteristically methylated among different tumor groups: *ADRA1D*, *MGMT*, *VHL*, and *THBS1*, and performed cluster analysis using the methylation average of 4 genes. As shown in Figure 2B, CCSK, RTK, and ESFT were successfully classified according to the DNA methylation pattern of these genes, suggesting that the DNA methylation analysis of these 4 genes is sufficient for the differential diagnosis of these tumors.

Since *THBS1* was found to be characteristically hypermethylated in CCSK (Figure 2B), we next examined whether the hypermethylation of *THBS1* alone can distinguish CCSK from other tumor groups. To confirm the specificity of *THBS1* hypermethylation in CCSK among pediatric renal tumors, we additionally analyzed Wilms' tumor and CMN. As shown in Figure 3, when we analyzed 6 each of RTK, CCSK, ESFT, and NK as well as 21 cases of Wilms' tumor and 9 cases of CMN, the CpG sites of *THBS1* were unmethylated in all of the cases, indicating that the CpG sites of *THBS1* are specifically hypermethylated in CCSK among pediatric renal tumors.

To detect the methylation of *THBS1* more easily, we have developed combined bisulfite restriction analysis (COBRA) and analyzed 21 cases of CCSK and 41 cases of Wilms' tumor, 6 cases of RTK, 9 cases of CMN, and 6 cases of NK. As shown in Figure 4 and Table 4, the digestion of bisulfite PCR products with HpyCH4IV clearly indicated that a CpG site of *THBS1* in all CCSK cases was hypermethylated. However, none of other tumor groups exhibited hypermethylation of the CpG site of *THBS1*. The results strongly indicate that hypermethylation of *THBS1* is a specific characteristic of CCSK among pediatric renal tumors, and could be utilized as diagnostic maker of this tumor.

Discussion

In this study, we carried out a DNA methylation analysis to identify genes differentially methylated in a series of pediatric tumors and we clearly showed that different pediatric sarcomas occurring in the kidney possess a distinct DNA methylation profile. Especially, CCSK is more frequently hypermethylated, but less hypomethylated, at the CpG island, compared with other tumors. Since pediatric renal sarcomas have overlapping morphologic and clinical features, the significant differences in epigenetic characteristics between these tumors are of particular interest and may represent the distinction of their cell origin or developmental mechanism. We also showed that these tumors can definitely be classified based on the DNA methylation profile, indicating the usefulness of epigenetic profiling for the differential diagnosis of

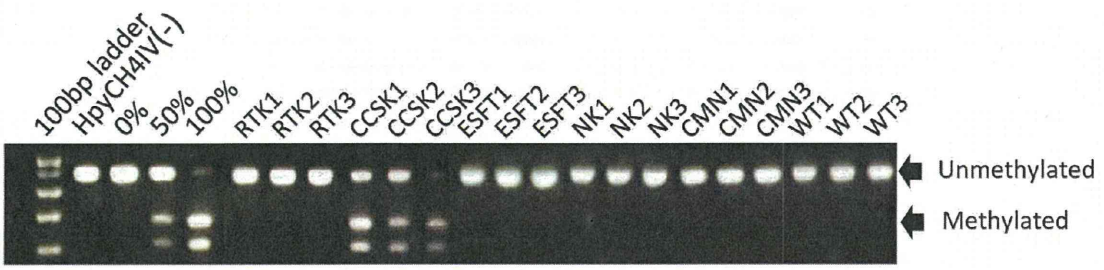

Figure 4. Combined bisulfite restriction analysis (COBRA) of *THBS1* in pediatric renal tumors. Using the same PCR products as in Figure 3, COBRA analysis was performed by digesting with the HpyCH4IV enzyme. The HpyCH4IV site is equivalent to CpG18 (chr15:37,660,642-37,660,645/hg18) in Figure 3. The positions of bands representing methylated and unmethylated DNA are indicated by arrows. As the control of HpyCH4IV digestion, 0, 50, and 100% methylated DNA were loaded on the same gel. WT: Wilms' tumor.
doi:10.1371/journal.pone.0062233.g004

Table 4. Frequency of *THBS1* methylation by COBRA.

	Hypermethylated cases
RTK	0/6
CCSK	21/21
ESFT	0/6
CMN	0/6
Wilms	0/41
NK	0/6

doi:10.1371/journal.pone.0062233.t004

pediatric renal sarcomas, and found that a combination of four genes is sufficient. Furthermore, the DNA methylation status of the *THBS1* CpG site detected by COBRA alone can distinguish CCSK cases from other pediatric renal tumors, including Wilms' tumor and CMN.

The pathological diagnoses of pediatric renal tumors are often supported by immunohistochemical and molecular genetic findings. For example, biallelic inactivation of *SMARCB1* as evidenced by negative immunohistochemical staining has high sensitivity and specificity for the diagnosis of RTK, and *ETV6-NTRK3* fusion is a marker for CMN of the cellular type. In the case of CCSK, however, it has neither immunohistochemical nor molecular genetic markers, while *YWHAE-FAM22* fusion was reported in only a minority [19]. Since *THBS1* hypermethylation is highly specific for CCSK, as we presented in this study, this finding should be useful for a molecular marker of this tumor. Especially, COBRA of the *THBS1* CpG site is highly accurate, reproducible, and can be performed without particular equipment, and, thus, it could be a candidate for routine examination for the differential diagnosis of CCSK from other pediatric renal tumors.

DNA methylation has been proposed as a diagnostic marker for certain cancers. For example, Goto reported that malignant mesothelioma could be differentiated from lung adenocarcinoma by methylation profiles [20], and Mahoney reported that embryonal and alveolar subtypes of rhabdomyosarcoma have a distinct DNA methylation profile [21]. In their cases, however, the methylation status of at least several genes was required for the differentiation of only two entities. In contrast, our findings showed that hypermethylation of a single locus of *THBS1* is sufficient for the differentiation of CCSK from other pediatric tumors and it could serve as a robust diagnostic marker for this tumor.

Hypermethylation of the *THBS1* CpG site has been observed in some tumors. For example, Guo et al. reported that the rate of methylation of *THBS1* was significantly higher in gastric cardia adenocarcinoma than that in the corresponding normal tissues and accompanied by reduction of its mRNA and protein expressions [22], and Guerrero et al. also reported that the hypermethylation of *THBS1* is associated with a poor prognosis in penile squamous cell carcinoma [23]. In both cases, the hypermethylation of *THBS1* has been suggested to be correlated with the pathogenesis.

THBS1 is a member of the thrombospondin family, and is known for putative antiangiogenic factor [24,25]. By employing a knockout mouse model, several studies have shown that the absence of *THBS1* leads to increased vascularization and THBS1 protein inhibits tumor progression in several ways, including direct effects on cellular growth and apoptosis in the stromal compartment [26–29]. Since CCSK is known to be rich in a fine vascular network, it is reasonable to presume that hypermethylation of the *THBS1* CpG site is involved in the pathogenesis of CCSK. However, we observed no significant correlations between the methylation status and expression of THBS1 by realtime RT-PCR and immunohistochemistry (data not shown). This is possibly due to hypermethylated CpG sites of *THBS1* in CCSK that we identified as not being responsible for *THBS1* expression, and other CpG sites are related to the regulation of *THBS1* expression. In fact, other CpG probes (cg19570574: chr15: 37660116–37660117/hg18, cg04051458: chr15: 37660352–37660353/hg18) in the upstream region of the *THBS1* transcription start site were hypomethylated in CCSK based on our assay. Another possibility is that THBS1 is expressed in a limited period during tumorigenesis. Further studies to elucidate the biological significance of CCSK hypermethylation are now underway.

In conclusion, pediatric renal sarcomas possess a distinct DNA methylation profile in a tumor-type-specific manner. The DNA methylation status of the *THBS1* CpG site detected by COBRA alone is sufficient for the distinction of CCSK from other pediatric renal tumors. Although further analysis to elucidate the biological importance of the differential DNA methylation of each tumor is required, our observation should shed light on the significance of the epigenetic diversity of pediatric renal tumors on their biological features and mechanism of pathogenesis.

Supporting Information

Figure S1 Images of frozen tissue sample by H.E. staining. Frozen tumor tissues were embedded in OCT-compound and sectioned in 6 μm, stained with H.E. The proportion of viable tumor tissue was evaluated under light microscope.
(TIF)

Figure S2 Correlation of the methylation values between Infinium assay and MassARRAY. In cases of *THBS1* and *CREG1*, methylation values of same CpG site measured by MassARRAY (average of 6 samples) and Infinium BeadChip Assays (average of 3 samples) were indicated in the scattergrams and values of coefficient of determination (R^2) were calculated. In case of *VHL*, two probe sites were shown. Since each site of *VHL* could not be discriminated from the neighbouring site by MassARRAY, the methylation value was obtained as an average of two sites. Coefficient of determination between the values obtained by two methods was larger than 0.99 in each case. Methylation levels of the equivalent CpG sites were correlated between Infinium assay and MassARRAY.
(TIF)

Figure S3 MassARRAY analysis of *VHL* in pediatric renal tumors. MassARRAY analysis of the *VHL* was carried out in 6 each of RTK, CCSK, ESFT, NK. Different colored of circles mark the position of CpG within the sequence (straight line) and the levels of methylation are shown in color (red, low methylation level; yellow, high methylation level). Gray circles represent the unanalyzed CpG sites. CpG5 and CpG13 are equivalent to Infinium assay probes.
(TIF)

Figure S4 Combined bisulfite restriction analysis (COBRA) of *VHL* in pediatric renal tumors. Bisulfite PCR amplification of *VHL* was carried out by using same primer for MassArray. COBRA analysis was performed by digesting with the TaqI restriction enzyme. The TaqI site is equivalent to CpG3 in MassARRAY analysis. The site of genome sequence is CCGA, which is converted to TaqI sequence (tCGA) by bisulfite reaction. PCR amplification of RTK4 was failed. The digested DNA was

separated on 2% agarose gels in 1×TAE buffer, stained with ethidium bromide, and visualized on a UV transilluminator. (TIF)

Table S1 Numbers of probes filtered with p-value and SD. (DOCX)

Acknowledgments

We thank Keiko Nakasato for technical assistance.

Author Contributions

Conceived and designed the experiments: HU HO NK. Performed the experiments: HU HO SA KN. Analyzed the data: HU HO. Contributed reagents/materials/analysis tools: HO JF JH MF KN KH. Wrote the paper: HU HO KK NK.

References

1. Eble JN, Sauter G, Epstein JI, Sesterhenn IA (2004) World Health Organization Classification of Tumours: Pathology and Genetics of Tumours of the Urinary System and Male Genital Organs. Lyon: IARC Press. p48–61.
2. Rubin BP, Chen CJ, Morgan TW, Xiao S, Grier HE, et al. (1998) Congenital mesoblastic nephroma t(12;15) is associated with ETV6-NTRK3 gene fusion: cytogenetic and molecular relationship to congenital (infantile) fibrosarcoma. Am J Pathol. 153: 1451–1458.
3. Argani P, Perlman EJ, Breslow NE, Browning NG, Green DM, et al. (2000) Clear cell sarcoma of the kidney: a review of 351 cases from the National Wilms Tumor Study Group Pathology Center. Am J Surg Pathol 24: 4–18.
4. Versteege I, Sevenet N, Lange J, Rousseau-Merck MF, Ambros P, et al. (1998) Truncating mutations of hSNF5/INI1 in aggressive pediatric cancer. Nature 394: 203–206.
5. Biegel JA, Tan L, Zhang F, Wainwright L, Russo P, et al. (2002) Alterations of the hSNF5/INI1 gene in central nervous system atypical teratoid/rhabdoid tumors and renal and extrarenal rhabdoid tumors. Clin Cancer Res 8: 3461–3467.
6. Imbalzano AN, Jones SN (2005) Snf5 tumor suppressor couples chromatin remodeling, checkpoint control, and chromosomal stability. Cancer Cell 7: 294–295.
7. Beckwith JB (1994) Renal neoplasms of childhood. 2nd ed. In: Sternberg SS, editor. Diagnostic surgical pathology. New York: Raven Press. 1741–1766.
8. Schuster AE, Schneider DT, Fritsch MK, Grundy P, Perlman EJ (2003) Genetic and genetic expression analyses of clear cell sarcoma of the kidney. Lab Invest 83: 1293–1299.
9. Baylin SB, Belinsky SA, Herman JG (2000) Aberrant methylation of gene promoters in cancer–concepts, misconcepts, and promise. J Natl Cancer Inst 92: 1460–1461.
10. Feinberg AP, Tycko B (2004) The history of cancer epigenetics. Nat Rev Cancer 4: 143–153.
11. Esteller M. (2002) CpG island hypermethylation and tumor suppressor genes: a booming present, a brighter future. Oncogene 21: 5427–5440.
12. Herman JG, Baylin SB (2003) Gene silencing in cancer in association with promoter hypermethylation. N Engl J Med 349: 2042–2054.
13. Anglesio MS, Evdokimova V, Melnyk N, Zhang L, Fernandez CV, et al. (2004) Differential expression of a novel ankyrin containing E3 ubiquitin-protein ligase, Hace1, in sporadic Wilms' tumor versus normal kidney. Hum Mol Genet. 13(18): 2061–2074.
14. Haruta M, Matsumoto Y, Izumi H, Watanabe N, Fukuzawa M, et al. (2008) Combined BuR1 protein down-regulation and RASSF1A hypermethylation in Wilms tumors with diverse cytogenetic change. Mol Carcinog. 47(9): 660–666.
15. Szemes M, Dallosso AR, Melegh Z, Curry T, Li Y, et al. (2013) Control of epigenetic states by WT1 via regulation of de novo DNA methyltransferase 3A. Hum Mol Genet. 22(1): 74–83.
16. Chilukamarri L, Hancock AL, Malik S, Zabkiewicz J, Baker JA, et al. (2007) Hypomethylation and aberrant expression of the glioma pathogenesis-related 1 gene in Wilms tumors. Neoplasia. (11): 970–978.
17. Esteller M, Herman JG (2004) Generating mutations but providing chemosensitivity: the role of O6-methylguanine DNA methyltransferase in human cancer. Oncogene. 23(1): 1–8.
18. Yu J, Ni M, Xu J, Zhang H, Gao B, et al. (2002) Methylation profiling of twenty promoter-CpG islands of genes which may contribute to hepatocellular carcinogenesis. J.BMC Cancer. 2: 29.
19. O'Meara E, Stack D, Lee CH, Garvin AJ, Morris T, et al. (2012) Characterization of the chromosomal translocation t(10;17)(q22;p13) in clear cell sarcoma of kidney. J Pathol. 227(1): 72–80.
20. Goto Y, Shinjo K, Kondo Y, Shen L, Toyota M, et al. (2009) Epigenetic profiles distinguish malignant pleural mesothelioma from lung adenocarcinoma. Cancer Res. 69(23): 9073–9082.
21. Mahoney SE, Yao Z, Keyes CC, Tapscott SJ, Diede SJ (2012) Genome-wide DNA methylation studies suggest distinct DNA methylation patterns in pediatric embryonal and alveolar rhabdomyosarcomas. Epigenetics 7(4): 400–408.
22. Guo W, Dong Z, He M, Guo Y, Guo J, et al. (2010) Aberrant methylation of thrombospondin-1 and its association with reduced expression in gastric cardia adenocarcinoma. J Biomed Biotechnol 721485 Epub 2010 Mar 15.
23. Guerrero D, Guarch R, Ojer A, Casas JM, Ropero S, et al.(2008)Hypermethy-)Hypermethylation of the thrombospondin-1 gene is associated with poor prognosis in penile squamous cell carcinoma. BJU Int. 102: 747–755.
24. Lawler J (2002) Thrombospondin-1 as an endogenous inhibitor of angiogenesis and tumor growth. J Cell Mol Med 6: 1–12.
25. Folkman J (2004) Endogenous angiogenesis inhibitors. APMIS 112: 496–507.
26. Greenaway J, Lawler J, Moorehead R, Bornstein P, Lamarre J, et al.(2007) Thrombospondin-1 inhibits VEGF levels in the ovary directly by binding and internalization via the low density lipoprotein receptor-related protein-1 (LRP-1). J Cell Physiol 210: 807–818.
27. Wang S, Wu Z, Sorenson CM, Lawler J, Sheibani N (2003) Thrombospondin-1-deficient mice exhibit increased vascular density during retinal vascular development and are less sensitive to hyperoxia-mediated vessel obliteration. Dev Dyn 228: 630–642.
28. Lawler J, Miao WM, Duquette M, Bouck N, Bronson RT, et al. (2001) Thrombospondin-1 gene expression affects survival and tumor spectrum of p53-deficient mice. Am J Pathol 159: 1949–1956.
29. Sund M, Hamano Y, Sugimoto H, Sudhakar A, Soubasakos M, et al. (2005) Function of endogenous inhibitors of angiogenesis as endothelium-specific tumor suppressors. Proc Natl Acad Sci USA 102: 2934–2939.

Pediatr Blood Cancer 2014;61:760–762

BRIEF REPORT
Two Cases of Neuroblastoma Comprising Two Distinct Clones

Fumito Yamazaki, MD,[1] Atsuko Nakazawa, MD, PhD,[2] Tomoo Osumi, MD,[1] Naoki Shimojima, MD, PhD,[3] Takeo Tanaka, MD, PhD,[4] Akira Nakagawara, MD, PhD,[5] and Hiroyuki Shimada, MD, PhD[1]*

We report two cases of high-risk metastatic neuroblastoma, comprising two biologically distinct components in the adrenal primary tumor, which showed clear differences not only histologically but also in *MYCN* amplification and *HA-RAS/TRKA* immunoreactivity (Case 1), anaplastic lymphoma kinase (ALK) immunoreactivity (Case 2). These two cases with multiple separated components were similar to cases classified as ganglioneuroblastoma, nodular subtype (GNBn), in terms of composite tumor. Comparable to the GNBn category, the prognosis of the patients described here may depend on the components with unfavorable histology according to International Neuroblastoma Pathology Classification. Further analyses of such composite neuroblastoma cases are important for assessing disease prognosis. Pediatr Blood Cancer 2014;61:760–762. © 2013 Wiley Periodicals, Inc.

Key words: ganglioneuroblastoma; international neuroblastoma pathology classification; neuroblastoma

INTRODUCTION

The International Neuroblastoma Pathology Classification (INPC) classifies peripheral neuroblastic tumors into four categories: neuroblastoma (Schwannian stroma-poor); ganglioneuroblastoma, intermixed (Schwannian stroma-rich); ganglioneuroma (Schwannian stroma-dominant); and ganglioneuroblastoma, nodular (GNBn) (composite: Schwannian stroma-rich/stroma-dominant, and stroma-poor) [1,2]. Among these four categories, only GNBn tumors are defined as composite tumors comprising histologically and biologically different clones. By definition, one of the tumor components in GNBn has features consistent with ganglioneuroblastoma, intermixed or ganglioneuroma, and the other has an appearance of neuroblastoma. Here, we report two cases of neuroblastoma comprising two histologically and biologically distinct clones, similar to the GNBn category in terms of having two or more different clones. However, this type of composite neuroblastoma could not be classified according to the current INPC system.

CASE PRESENTATION

Case 1. A 14-month-old male presented with intermittent fever for 2 months. Abdominal computed tomography (CT) revealed an approximately 4-cm left adrenal mass. After complete resection of the mass, he was diagnosed with neuroblastoma. Other sites of involvement included the lymph nodes and bone marrow: International Neuroblastoma Risk Group Classification (INRG) stage M. After surgery, the patient underwent induction/high-dose chemotherapy with autologous peripheral blood stem cell transplantation, radiation, and 13-cis-retinoic acid treatment. Complete remission has been maintained for 3 years since diagnosis.

Microscopically, the resected left adrenal gland tumor comprised two neuroblastoma nodular components separated by a fibrillary matrix (components A and B in Fig. 1a). Component A was classified as neuroblastoma, a poorly differentiated subtype with a high mitosis-karyorrhexis index (MKI); small round cells with almost bare nuclei surrounded by a few neuropils were observed (Fig. 1b). Component B was classified as neuroblastoma, poorly differentiated subtype with a low MKI; relatively large nuclear cells surrounded by abundant neuropils were observed. Component B was more differentiated compared with component A. Some cells in component B had abundant eosinophilic cytoplasm and were observed to be in the process of differentiating into ganglion cells (Fig. 1c). Schwannian cells were not identified by S-100 immunostaining in both component A and B. Lymph nodes around the left adrenal tumor and bone marrow contained metastatic tumor cells similar in appearance to component A cells. According to INPC, component A was classified into Unfavorable Histology Group and component B into Favorable Histology Group.

For each of the two components observed in the case, fluorescent in situ hybridization (FISH) using the LSI *MYCN* (2p24) SpectrumGreen/CEP 2 Spectrum Orange Probe (Vysis) was performed on formalin-fixed, paraffin-embedded material, and *HA-RAS/TRKA* expression patterns were immunohistochemically examined. Component A exhibited *MYCN* amplification and low *HA-RAS/TRKA* expression, whereas component B demonstrated *MYCN* non-amplification and high *HA-RAS/TRKA* expression. In contrast, array-based comparative genomic hybridization profiles of two components demonstrated similar patterns for chromosomal events as a prognostic marker, including deletions of chromosomes 1p and 11q and gain of chromosome 17q. *MYCN* amplification was presented only in component A, which was the same as shown in FISH analysis. Both components were classified within the genetic group of partial chromosomal gains and/or losses that indicate poor disease prognosis [3].

Case 2. A 21-month-old male presented with right hip pain and gradual bulging of his eyes for several days. Abdominal CT showed an approximately 8-cm right adrenal mass. He was diagnosed with

[1]Department of Pediatrics, Keio University School of Medicine, Tokyo, Japan; [2]Department of Pathology, National Medical Center for Child Health and Development, Tokyo, Japan; [3]Department of Pediatric Surgery, Keio University, School of Medicine, Tokyo, Japan; [4]National Hospital Organization Hiroshimanishi Medical Center, Hiroshima, Japan; [5]Department Division of Biochemistry, Chiba Cancer Center Research Institute, Chiba, Japan

Conflict of interest: Nothing to declare.

*Correspondence to: Hiroyuki Shimada, Department of Pediatrics, Keio University School of Medicine, 35 Shinanomachi, Shinjuku-ku, Tokyo 160-8582, Japan. E-mail: hshimada@a5.keio.jp

Received 4 July 2013; Accepted 22 August 2013

DOI 10.1002/pbc.24779
Published online 20 September 2013 in Wiley Online Library (wileyonlinelibrary.com).

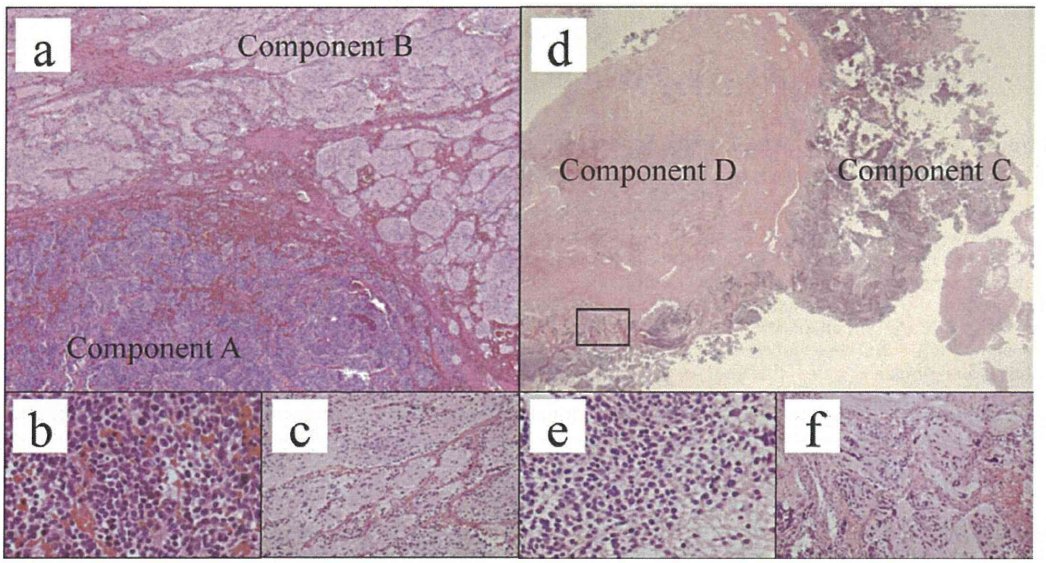

Fig. 1. **a**: The resected tumor in the left adrenal gland comprised two distinct components: component A (lower) and component B (upper). Case 1, H&E, 40×. **b**: Component A: neuroblastoma, a poorly differentiated subtype with a high mitosis-karyorrhexis index (MKI). H&E, 400×. **c**: Component B: neuroblastoma, a poorly differentiated subtype with a low MKI, more differentiated compared with component A.H&E, 400×. **d**: The tissue obtained at biopsy in the right adrenal gland comprised two distinct components: component C (right) and component D (left). Most Component D consisted of fibrous tissue with small foci of neuroblasts. A portion of Component D (square, Figure f) was classified as neuroblastoma, a differentiating subtype. Case 2, H&E, 40×. **e**: Component C: neuroblastoma, a poorly differentiated subtype with a high MKI. H&E, 400×. **f**: Component D: neuroblastoma, a differentiating subtype. H&E, 400×.

neuroblastoma following biopsy of the mass. Other sites of involvement included the lymph nodes, multiple bones, and bone marrow (INRG stage M). Because of the poor response to multidrug chemotherapy, a tandem transplantation was planned after abdominal tumor resection. Unfortunately, the patient died from sudden respiratory failure before the second transplantation.

Microscopically, the tissue obtained by biopsying the right adrenal gland before treatment comprised two neuroblastoma nodular components separated by a fibrillary matrix (components C and D in Fig. 1d). Component C was classified as neuroblastoma, a poorly differentiated subtype with a high MKI (Fig. 1e). Most of component D consisted of fibrous tissue with small foci of neuroblasts. A portion of component D was classified as neuroblastoma, a differentiating subtype. MKI could not be assessed because the number of neuroblastic cells was insufficient (<5,000 cells; Fig. 1f). Schwannian cells were not identified by S-100 immunostaining in both component C and D. Lymph nodes around the right adrenal tumor and bone marrow contained metastatic tumor cells similar in appearance to the cells of component C. According to INPC, component C was classified into Unfavorable Histology Group and component D into Favorable Histology Group. Both components exhibited *MYCN* non-amplification and high *HA-RAS/TRKA* expression. However, different patterns were observed in ALK expression analysis; components C and D showed high and low ALK immunoreactivity, respectively.

DISCUSSION

We present two cases of neuroblastoma comprising two histologically and biologically distinct neuroblastoma components. A similar case was previously reported by Sano et al. [4]; one component showed neuroblastoma, poorly differentiated subtype with a high MKI and *MYCN* amplification, whereas the other showed neuroblastoma, poorly differentiated subtype with a low MKI and *MYCN* non-amplification. INPC distinguished the two components into Unfavorable and Favorable Histology Groups. In addition to clear histological differences between the two components in Sano's case and our two cases, the components differed in *MYCN* amplification in Sano's case, *MYCN* amplification and *HA-RAS/TRKA* immunoreactivity in our Case 1, and ALK immunoreactivity in our Case 2. Similar to *MYCN* amplification and *Ha-ras/trkA* gene expression [5], ALK immunoreactivity is a significant predictor of disease prognosis [6,7]. These three cases indicate that the combination of two separate neuroblastoma components that histologically, immunohistochemically, and biologically vary depending on a case-by-case basis.

Our two cases were similar to tumors classified as GNBn in that they also showed multiple separated components (clones). Based on the similarity with GNBn, we propose describing the composite neuroblastomas reported here as neuroblastoma, nodular (NBn), as previously proposed by Sano et al. [4]. Nonaggressive components (ganglioneuroblastoma, intermixed or ganglioneuroma) of GNBn are classified as Favorable Histology in INPC and are considered to have differentiated from neuroblastoma based on the age-linked maturational sequence. If we can observe a GNBn tumor at an earlier age, the nonaggressive components may have the appearance of neuroblastoma with Favorable Histology in the first or second step of the age-linked maturational sequence, that is, poorly differentiated or differentiating neuroblastoma. This subtype is considered to correspond to NBn (Fig. 2).

Patients with GNBn can be divided into two prognostic subsets by applying the same age-linked morphological criteria used in

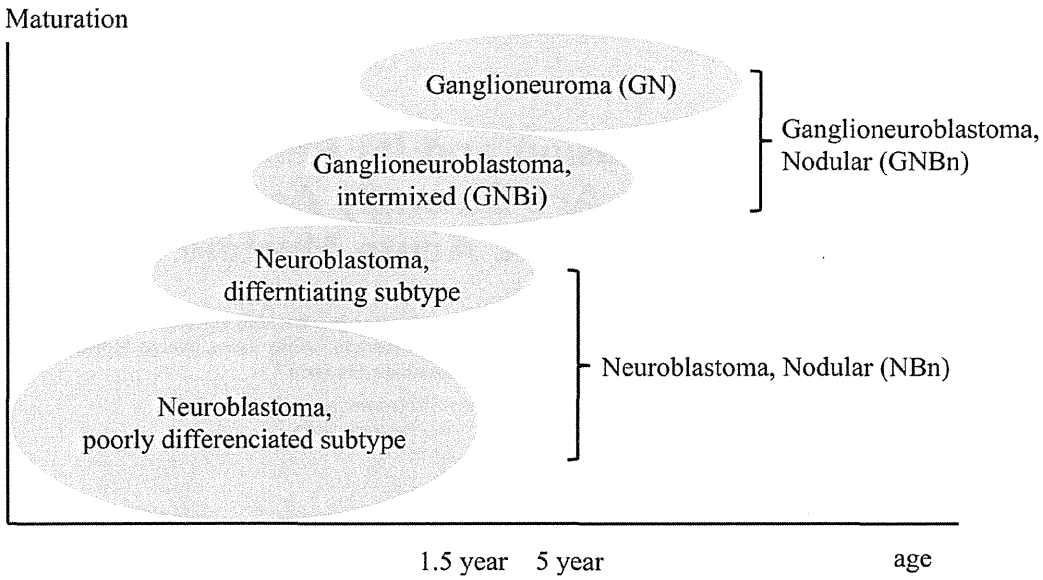

Fig. 2. The nonaggressive components classified as Favorable Histology of composite neuroblastic tumors (ganglioneuroblastoma, nodular (GNBn) and Neuroblastoma, nodular (NBn)) are considered to differentiate from poorly differentiated (<1.5 years of age at diagnosis) to differentiating (<5 years of age) neuroblastomas to ganglioneuroblastoma, intermixed and to ganglioneuroma based on the age-linked maturational sequence. Ganglioneuroblastoma, intermixed or ganglioneuroma are the feature of nonaggressive components in GNBn, while poorly differentiated or differentiating neuroblastoma are the feature of those in NBn.

neuroblastoma category to their neuroblastoma components: favorable and unfavorable subsets. The difference in estimated survival between these two subsets of GNBn patients is statistically significant [8]. Therefore, the INPC system was modified to account for this difference [9]. If the same principle is applied, NBn patient prognosis should depend on the components with unfavorable histology. Although histological and molecular intratumoral heterogeneity was previously reported in neuroblastoma with transition from one component to the other [10,11], two different tumor components (Favorable and Unfavorable Histology Groups) were clearly distinguishable and separately identifiable in NBn, including our cases. *MYCN* analysis by FISH with paraffin sections and immunohistochemical analysis for ALK were critical for precisely identifying the two histologically and biologically different neuroblastoma components. Further analyses of NBn patients are needed to assess disease prognosis by obtaining a sufficient amount of tumor tissues for precise phenotypic and genotypic evaluations.

REFERENCES

1. Shimada H, Ambros IM, Dehner LP, et al. The international neuroblastoma pathology classification (the Shimada system). Cancer 1999;86:364–372.
2. Shimada H, Ambros IM, Dehner LP, et al. Terminology and morphologic criteria of neuroblastic tumors: Recommendations by the International Neuroblastoma Pathology Committee. Cancer 1999;86:349–363.
3. Ohira M, Nakagawara A. Global genomic and RNA profiles for novel risk stratification of neuroblastoma. Cancer Sci 2010;101:2295–2301.
4. Sano H, Gonzalez-Gomez I, Wu SQ, et al. A case of composite neuroblastoma composed of histologically and biologically distinct clones. Pediatr Dev Pathol 2007;10:229–232.
5. Kyo Y, Tanaka T, Hayashi K, et al. Identification of therapy-sensitive and therapy-resistant neuroblastoma subtypes in stages III, IVs and IV. Cancer Lett 2011;1:27–33.
6. Duijkers FA, Gaal J, Meijerink JP, et al. High anaplastic lymphoma kinase immunohistochemical staining in neuroblastoma and ganglioneuroblastoma is an independent predictor of poor outcome. Am J Pathol 2012;180:1223–1231.
7. Passoni L, Longo L, Collini P, et al. Mutation-independent anaplastic lymphoma kinase overexpression in poor prognosis neuroblastoma patients. Cancer Res 2009;69:7338–7346.
8. Umehara S, Nakagawa A, Matthay KK, et al. Histopathology defines prognostic subsets of ganglioneuroblastoma, nodular. Cancer 2000;89:1150–1161.
9. Peuchmaur M, d'Amore ES, Joshi VV, et al. Revision of the international neuroblastoma pathology classification: Confirmation of favorable and unfavorable prognostic subsets in ganglioneuroblastoma, nodular. Cancer 2003;98:2274–2281.
10. Ambros PF, Ambros IM, Kerbl R, et al. Intratumoral heterogeneity of 1p deletions and MYCN amplification in neuroblastomas. Med Pediatr Oncol 2001;36:1–4.
11. Thorner PS, Ho M, Chilton-MacNeill S, et al. Use of chromogenic in situ hybridization to identify MYCN gene copy number in neuroblastoma using routine tissue sections. Am J Surg Pathol 2006;30:635–642.